MICHIGAN STATE UNIVERSITY

CYCLOTRON LABORATORY

COMPARISON OF NON-COMPOUND NEUTRON AND PROTON EMISSION IN ^{16}O INDUCED REACTIONS ON ^{238}U AT 310 MeV

J. KASAGI, S. SAINI, T.C. AWES, A. GALONSKY,
C.K. GELBKE, G. POGGI, D.K. SCOTT, K.L. WOLF
and R.L. LEGRAIN

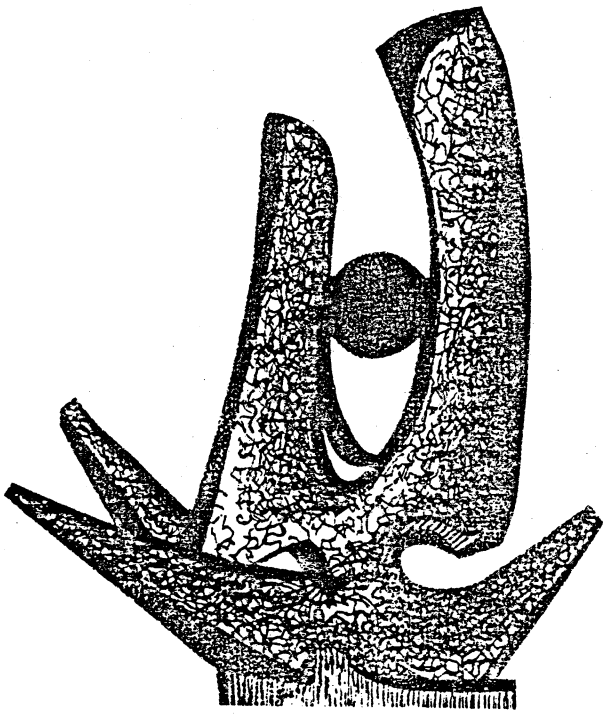

JULY 1981

MSUCL-352

MSUCL-352
July 1981

Comparison of non-compound neutron and proton emission in ^{16}O induced reactions on ^{238}U at 310 MeV

J. Kasagi, S. Saini,[+] T.C. Awes, A. Galonsky
C.K. Gelbke,[++] G. Poggi[+++] and D.K. Scott
Cyclotron Laboratory, Michigan State University
East Lansing, MI 48824, USA

and

K.L. Wolf
Chemistry Division, Argonne National Laboratory
Argonne, IL 60439, USA

and

R.L. Legrain[++++]
Lawrence Berkeley Laboratory
Berkeley, CA 94720, USA

[+] On leave from: Bhabha Atomic Research Center, India
[++] Alfred P. Sloan Fellow
[+++] On leave from University of Florence, Italy
[++++] On leave from C.E.N., Saclay, France

Abstract

The emission of energetic neutrons and protons in coincidence with fission fragments was measured for the reactions $^{238}U(^{16}O,nf)$ and $^{238}U(^{16}O,pf)$. Larger cross sections were observed for the emission of high-energy protons than for the emission of high-energy neutrons. The differences in spectral shapes and the implications for the coalescence model are discussed.

In the last few years, it has been established that the collision between complex nuclei at non-relativistic energies may lead to the emission of energetic light particles which cannot be explained in terms of evaporation from completely equilibrated nuclei.[1-10] Assuming that protons and neutrons have similar spectral shapes, it has been shown[11,12] that the energy spectra of deuterons and tritons may be related to the energy spectra of protons by a simple coalescence relation. However, a direct comparison of non-compound proton and neutron cross sections has not yet been performed. In this letter, we present the first such comparison; the reactions used were $^{238}U(^{16}O,pf)$ and $^{238}U(^{16}O,nf)$ at 310 MeV incident energy.

The experiment was performed at the 88-inch cyclotron of the Lawrence Berkeley Laboratory. A UF_4-target of thickness 320 $\mu g/cm^2$, mounted on an 80 $\mu g/cm^2$ carbon backing, was irradiated by $^{16}O^{6+}$ ions of 310 MeV incident energy. The target and fission detector were mounted in a thin-walled scattering chamber[13]

fabricated of aluminum. Fission fragments were detected with a surface barrier detector of 60 μm depletion depth and 450 mm^2 active area. This detector was mounted at an angle of $\theta_f = -90^o$ with respect to the beam axis and at a distance of 1.5 cm from the center of the target. Four liquid scintillation detectors (NE 213) of diameter and thickness 11.4 cm x 6.0 cm, 12.7 cm x 5.1 cm, 12.7 cm x 7.6 cm, and 12.7 cm x 7.6 cm were used to detect neutrons emitted at angles with respect to the beam of 25^o, 40^o, 55^o and 95^o respectively, in coincidence with fission fragments. The flight paths were 2.05 m. In order to reduce the background due to extraneous sources and due to scattering in the experimental vault, these detectors were placed inside shields constructed of lead, concrete and paraffin. The background remaining was determined by measurements with a tapered steel bar of 60 cm length halfway between the target and each detector. The bar absorbed the neutrons originating in the target but allowed extraneous neutrons to reach the detector. This background of about 10-15% of the total events was subtracted in the off-line analysis. Energetic charged particles were discriminated by an anticoincidence requirement with transmission-mounted solid state detectors placed outside the scattering chamber. Pulse shape information from each scintillator was obtained by means of Canberra Model 2160 pulse shape discriminators.[14]

In the second part of the experiment, coincident protons were detected with two ΔE-E telescopes positioned at angles of $\theta_p = 25^o$ and 55^o. These telescopes consisted of a 400 μm thick surface barrier detector and a 7.5 cm thick NaI (Tl) detector.

The detectors were placed outside the scattering chamber which had two exit ports covered with 50 μm thick mylar windows at these angles. The energy calibration of these detectors was established by observing 45-MeV protons elastically scattered from a gold target. The shapes of the high energy tails of the proton spectra measured in coincidence with fission fragments were consistent with previous measurements.[12]

Downscaled fission singles data were recorded simultaneously with the coincidence data. For each event, the pulse heights of all detector signals were recorded on magnetic tape; in addition, the time difference between light particle and fission detector signals was recorded together with the output of the pulse shape information circuit for the neutron detector. The final analysis, including particle identification, energy calibrations and corrections for random coincidences was performed off-line.

In the off-line analysis, two-dimensional gates were set in the pulse-height versus pulse-shape matrices to distinguish γ-rays from neutrons. The neutron detection efficiency was calculated with a modified version of a computer code originally developed by Kurz.[15] For a given detector thickness, the efficiency depends primarily on the threshold set on the pulse height distribution. The threshold for each detector was chosen to be higher than the electronic threshold, and two different values of threshold for each detector were tried to check the calculated efficiency. The accuracy of the absolute neutron efficiency is estimated to be ±15%. The neutron energy was determined from the flight-time. By correcting for the dependence of the neutron-fission timing signal on the measured energies of the fission

fragments, an overall time resolution of 1.0 nsec (fwhm) was achieved, corresponding to an energy resolution of 5 MeV (fwhm) at 50 MeV.

The differential neutron multiplicities per fission event, $d^2N/N_f dE d\Omega$, are shown in Fig. 1. At low energies, the spectra are dominated by a low temperature component which is not inconsistent with the statistical evaporation of neutrons from equilibrated target residues and fission fragments. A corresponding component is not apparent in the proton spectra.[11,12] At higher neutron energies the energy spectra fall off less rapidly with increasing energy than expected of statistical emission from fully equilibrated heavy nuclei. The high energy regions of the neutron spectra exhibit characteristics that are qualitatively similar to those observed for the emission of energetic charged particles: with increasing scattering angle the cross sections decrease and the energy spectra become steeper.

In order to facilitate the comparison of proton and neutron cross sections, we have decomposed each neutron spectrum into two components by fitting the energy spectra with the following function:

$$\frac{d^2N(E)}{N_f dE d\Omega} = N_o \, e^{-E/T_o} + N_1 \sqrt{E}\, e^{-E/T_1} \quad . \qquad (1)$$

The first term, which omits an energy factor, adequately represents the low energy component, and the second term describes the high energy component which we associate with preequilibrium processes; N_0, T_0, N_1, T_1 are adjustable parameters. This decomposition

is shown in Fig. 1 by the solid and dashed curves. The corresponding parameters are given in Table 1. The dotted lines included in the figure show the uncertainties within which the high energy regions of the neutron spectra are believed to be established. The limits defined by these dotted lines will be used for the comparison with the proton cross sections shown in Fig. 2.

The proton cross sections measured in this experiment are compared to the corresponding neutron cross sections in Fig. 2. The proton data are represented by solid points and the pre-equilibrium neutron components are given by the shaded areas in Fig. 2a. The shapes of the proton and neutron spectra exhibit significant differences. Steeper slopes are observed for the neutron spectra than for the proton spectra. At lower energies ($E \lesssim 30$ MeV) the neutron cross sections exceed the proton cross sections. However, the neutron cross section drops below the proton cross section at higher energies ($E \gtrsim 30$ MeV), a result which conflicts with the simple expectation[16] that the neutron-to-proton cross section ratio should scale with the neutron-to-proton ratio of the emitting system (be it projectile, target, or the composite system).

The differences between the low energy part of the proton and neutron spectra are most likely due to barrier penetration effects. To illustrate this point, we have transformed the neutron spectra of Fig. 2a according to the relation

$$\frac{d^2N^{(p)}(E)}{N_f dE d\Omega} = \frac{\sigma_R^{(p)}(E)}{\sigma_R^{(n)}(E)} \frac{d^2N^{(n)}(E)}{N_f dE d\Omega} \quad . \qquad (2)$$

In eq. (2), the inverse reaction cross sections are calculated from the optical model by using the potentials of ref. 17. The resulting cross sections are shown by the shaded areas in Fig. 2b. Reasonable agreement with the proton cross sections is obtained in the low energy region. The high energy part of the spectrum is, however, only slightly modified ($\sigma_R^{(p)} \simeq \sigma_R^{(n)}$ at high energies) and, as a consequence, the proton-to-neutron ratio at high energies is not affected by this procedure. We also want to point out that eq. (2) implies that the partial waves are added incoherently and have the same statistical weight as for the inverse reactions. These assumptions may not be correct; they will, however, affect the detailed shapes of the spectra only at low energies and not in the high energy tails.

Our observations show the qualitative trends predicted by recent precompound model calculations of Blann[18] for ^{16}O induced reactions on ^{197}Au at 214 MeV incident energy. The total number of preequilibrium neutrons is predicted to be larger than the total number of preequilibrium protons. In addition, a steeper slope is predicted for the (angle integrated) neutron spectrum than for the corresponding proton spectrum. This results in lower neutron cross sections in the high energy tail of the spectrum and larger neutron cross sections in the low energy part of the spectrum when compared to the proton spectrum. However, these qualitative features are not predicted by recent calculations[16] of nucleon emission from the interface of the two colliding nuclei ("hot spot" model).

Recently, it has been shown that the cross sections for the emission of energetic deuterons and tritons may be related to the proton cross sections by a simple coalescence relation.[11,12] This coalescence relation was derived[12] by making the simplifying assumption that the cross sections for pre-equilibrium proton and neutron emission are related by[12,19]

$$\frac{d^2\sigma_n(E)}{dE d\Omega} = \frac{N}{Z} \frac{d^2\sigma_p(E+Ec)}{dE d\Omega} \qquad (3)$$

In eq. (3), N/Z is the neutron-to-proton ratio of the compound nucleus. The energy shift E_c was introduced to correct for the final state Coulomb repulsion from the target nucleus. The physical picture behind eq. (3) is that protons and neutrons have identical kinetic energy distributions at the nuclear surface, where the observed complex particles are most likely to originate. The Coulomb field of the target nucleus merely displaces the energy spectrum of charged particles by the amount E_c. It is clear from Fig. 2a that eq. (3) is inconsistent with our observations. The shapes of the neutron spectra predicted from the proton cross sections would differ significantly from the measured neutron spectra. The coalescence calculations are quite sensitive to this low energy region; as a consequence, the deuteron cross sections are not given by the product of proton and neutron cross sections as determined in this experiment. The success of the coalescence relation given in ref. 12 and possible alternative explanations[20] for the formation of composite light particles remain an interesting subject for future investigations.

In summary, different shapes were observed for non-compound proton and neutron spectra in qualitative agreement with recent precompound model predictions.[18] The main differences in these shapes are likely to arise from the different barrier penetrabilities for protons and neutrons and, to a lesser extent, from final state interactions. The observed differences in proton and neutron cross sections make it difficult to understand the success of the coalescence model where these differences have not been taken into account. This problem also exists at relativistic energies where the proton and neutron spectra are also different.[21]

We want to express our gratitude to Dr. B.G. Harvey, Dr. R.G. Stokstad and the 88" cyclotron operating staff for their generous support of this experiment. This material is based upon work supported by the National Science Foundation under Grant No. PHY 78-22696 and in part by the Office of Basic Energy Sciences, Division of Nuclear Sciences, U.S. Department of Energy.

References

1. T. Inamura, M. Ishihara, T. Fukuda, T. Shimoda, and H. Hiruta, Phys. Lett. 68B (1977) 51.
2. L. Westerberg, D.G. Sarantites, D.C. Hensley, R.A. Dayras, M.L. Halbert, and J.H. Barker, Phys. Rev. C18 (1978) 796.
3. D.R. Zolnowski, H. Yamada, S.E. Cala, A.C. Kahler, and T.T. Sugihara, Phys. Rev. Lett. 41 (1978) 92.
4. T.C. Awes, C.K. Gelbke, B.B. Back, A.C. Mignerey, K.L. Wolf, P. Dyer, H. Breuer, and V.E. Viola, Jr., Phys. Lett. 87B (1979) 43.
5. K. Siwek-Wilczyńska, E.H. du Marchie van Voorthuysen, J. van Popta, R.H. Siemssen, and J. Wilczyński, Phys. Rev. Lett. 42 (1979) 1599, and Nucl. Phys. A330 (1979) 150.
6. T. Inamura, T. Kojima, T. Nomura, T. Sugitate, and H. Utsunomiya, Phys. Lett. 84B (1979) 71.
7. H. Yamada, D.R. Zolnowski, S.E. Cala, A.C. Kahler, J. Pierce, and T.T. Sugihara, Phys. Rev. Lett. 43 (1979) 605.
8. H. Utsunomiya, T. Nomura, T. Inamura, T. Sugitate, and T. Motobayashi, Nucl. Phys. A334 (1980) 127.
9. A. Gavron, R.L. Ferguson, F.E. Obenshain, F. Plasil, G.R. Young, G.A. Petitt, K.G. Young, D.G. Sarantites, and C.F. Maguire, Phys. Rev. Lett. 46 (1981) 8.
10. H. Gemmeke, P. Netter, Ax. Richter, L. Lassen, S. Lewandowski, W. Lücking, and R. Schreck, Phys. Lett. 97B (1980) 213.
11. T.C. Awes, C.K. Gelbke, G. Poggi, B.B. Back, B. Glagola, H. Breuer, V.E. Viola, Jr., and T.J.M. Symons, Phys. Rev. Lett. 45 (1980) 513.

12. T.C. Awes, G. Poggi, C.K. Gelbke, B.B. Back, B.G. Glagola, H. Breuer, V.E. Viola, Jr., Michigan State University Preprint MSUCL 343, 1980, and to be published in Phys. Rev. C.

13. D. Hilscher, J.R. Birkelund, A.D. Hoover, W.U. Schröder, W.W. Wilcke, J.R. Huizenga, A.C. Mignerey, K.L. Wolf, H.F. Breuer, and V.E. Viola, Jr., Phys. Rev. C20 (1979) 576.

14. P. Sperr, H. Spieler, M.R. Maier and D. Evers, Nucl. Instr. and Meth. 116 (1974) 55.

15. R.J. Kurz, UCRL-11339 (1964), unpublished.

16. W.W. Morison, S.K. Samaddar, D. Sperber and M. Zielińska-Pfabe, Phys. Lett. 93B (1980) 379.

17. F.D. Becchetti, Jr., and G.W. Greenlees, Phys. Rev. 182 (1969) 1190.

18. M. Blann, Phys. Rev. C23 (1981) 205.

19. M. Gyulassy and S.K. Kauffmann, Nucl. Phys. A362 (1981) 503.

20. F. Hachenberg, H.C. Chiang, and J. Hüfner, Phys. Lett. 97B (1980) 183.

21. W. Schimmerling, J.W. Kast, D. Ortendahl, R. Madey, R.A. Cecil, B.D. Anderson, and A.R. Baldwin, Phys. Rev. Lett. 43 (1979) 1985.

FIG. 1. Differential neutron multiplicities per fission event measured for the reaction $^{238}U(^{16}O,nf)$ at 310 MeV. The solid and dashed lines show the decomposition into equilibrium and non-equilibrium components, respectively. The dotted lines indciate the estimated errors within which the high energy regions of the neutron spectra are established. These limits are used for the comparison with the proton spectra in Fig. 2.

FIG. 2. Differential proton multiplicities per fission event measured for the reaction $^{238}U(^{16}O,nf)$ at 310 MeV. The shaded areas represent the measured preequilibrium neutron multiplities (part a) and their predicted transformation into proton multiplicities according to eq. 2 of the text (part b).

Table I. Parameters of eq. 1 used for the decomposition of equilibrium and non-equilibrium components shown in Fig. 1.

θ_n	$N_o(MeV \cdot sr)^{-1}$	$T_o(MeV)$	$N_1(MeV^{3/2} \cdot sr)^{-1}$	$T_1(MeV)$
25^o	1.35	2.45	0.036	7.60
40^o	1.85	2.35	0.025	7.4
55^o	2.00	2.20	0.024	6.2
95^o	1.78	1.85	0.038	4.0

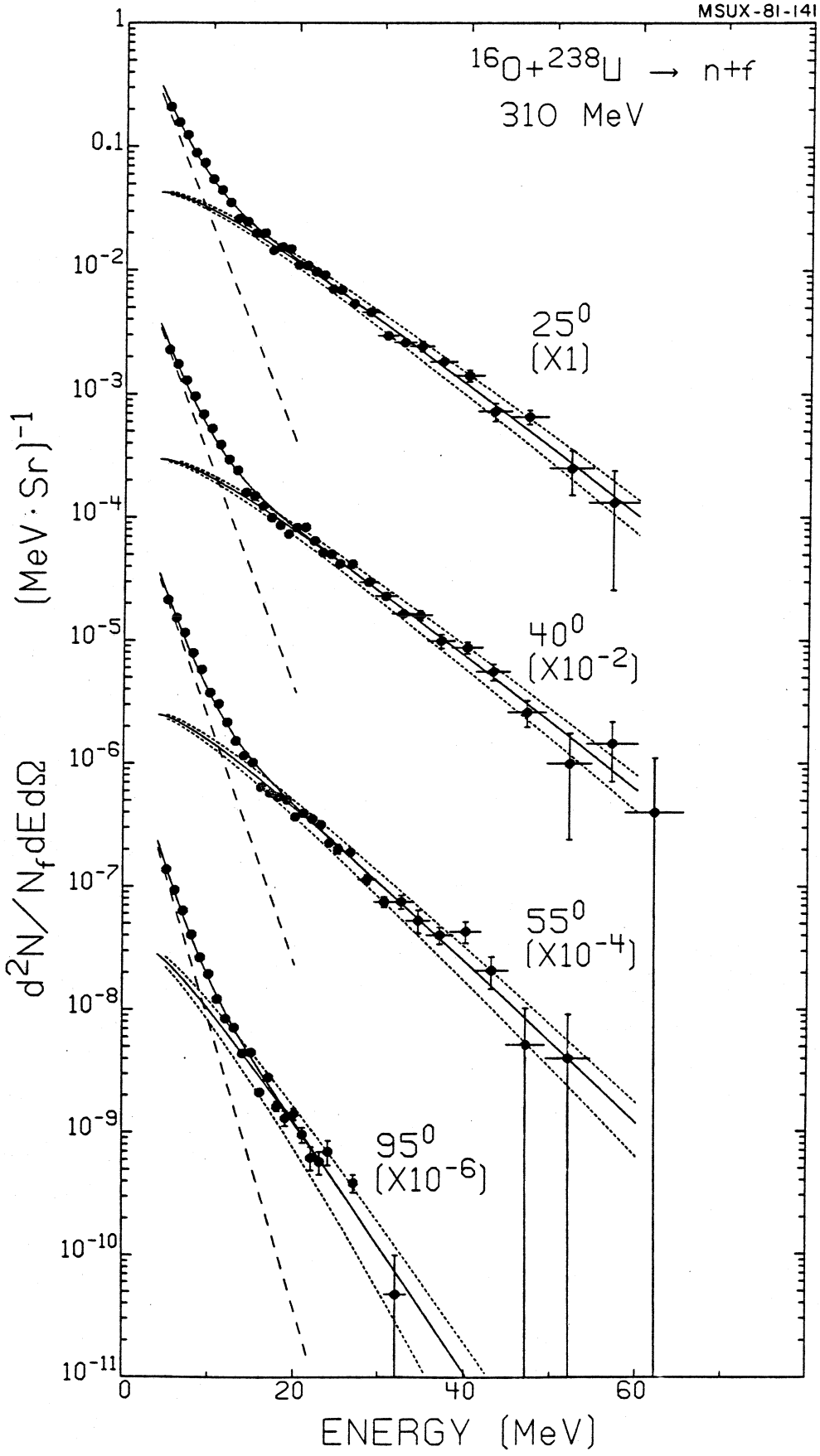
MSUX-81-141
$^{16}O+^{238}U \rightarrow n+f$
310 MeV
25^0
(X1)
40^0
$(X10^{-2})$
55^0
$(X10^{-4})$
95^0
$(X10^{-6})$
$d^2N/N_f dE d\Omega$ $(MeV \cdot Sr)^{-1}$
ENERGY (MeV)
1
0.1
10^{-2}
10^{-3}
10^{-4}
10^{-5}
10^{-6}
10^{-7}
10^{-8}
10^{-9}
10^{-10}
10^{-11}
0
20
40
60

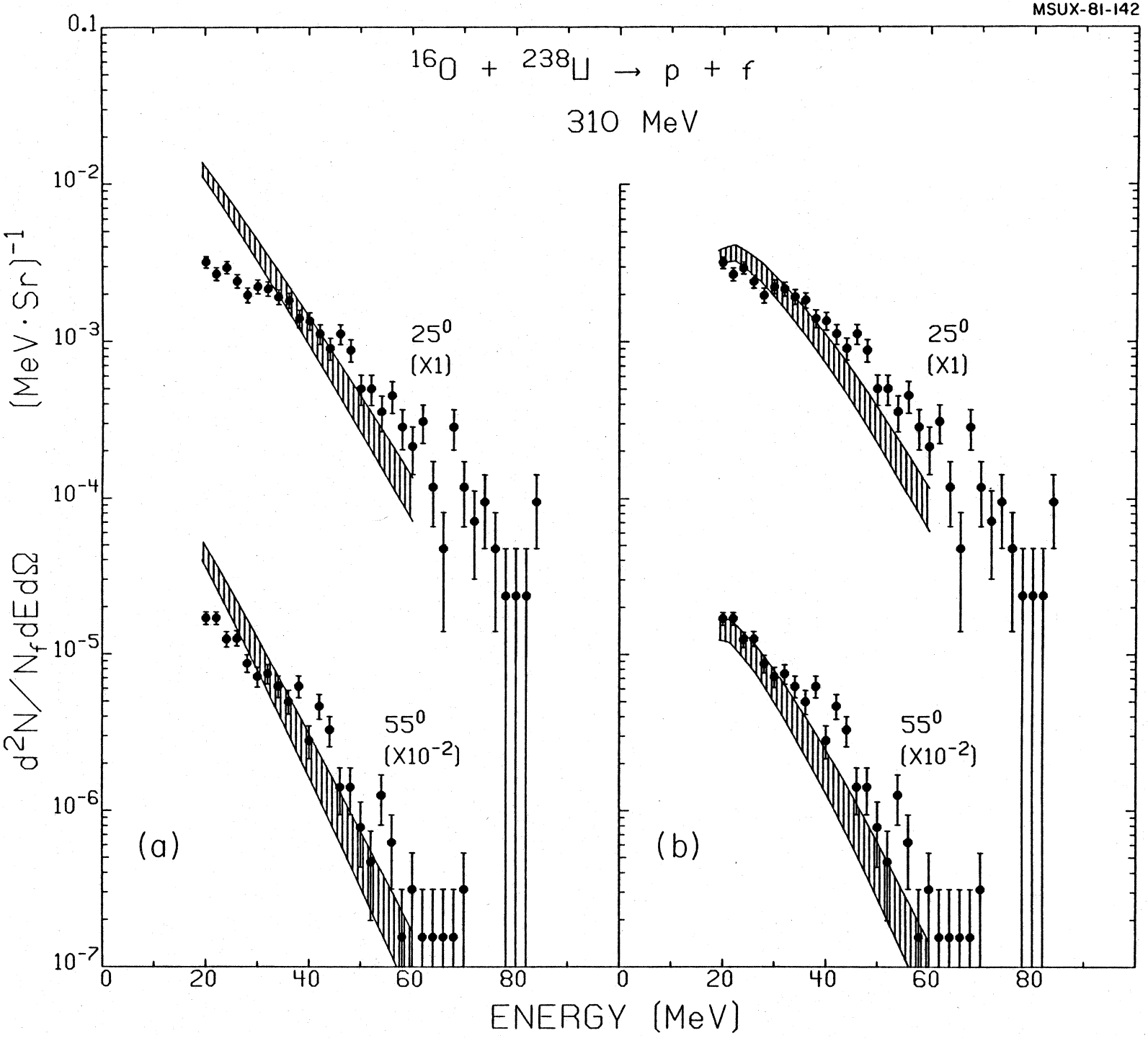
$^{16}O + ^{238}U \rightarrow p + f$
310 MeV
$d^2N/N_f dE d\Omega$ (MeV·Sr)$^{-1}$
25^0 (X1)
55^0 (X10^{-2})
(a)
(b)
ENERGY (MeV)
0.1
10^{-2}
10^{-3}
10^{-4}
10^{-5}
10^{-6}
10^{-7}
0
20
40
60
80